Atmos. Meas. Tech. Discuss., https://doi.org/10.5194/amt-2018-186
Manuscript under review for journal Atmos. Meas. Tech.
Discussion started: 20 June 2018

Atmospheric Measurement Techniques Discussions

The Advanced Infra-Red WAter Vapour Estimator (AIRWAVE) version 2: algorithm evolution, dataset description and performance improvements

Elisa Castelli[1], Enzo Papandrea[2,1], Alessio Di Roma[3], Bianca Maria Dinelli[1], Stefano Casadio[2], and Bojan Bojkov[4]

[1]Istituto di Scienze dell'Atmosfera e del Clima, ISAC-CNR, Via Gobetti 101, 40129 Bologna, Italy
[2]Serco s.p.a.,Via Sciadonna 24-26, 00044 Frascati, Italy
[3]Dipartimento di Fisica e Astronomia, DIFA, Universita' di Bologna, Viale Berti Pichat 6/2, 40127, Bologna, Italy
[4]EUMETSAT, Eumetsat Allee 1, D-64295 Darmstadt, Germany

Correspondence to: E. Castelli
(e.castelli@isac.cnr.it)

Abstract. The Total Column Water Vapour (TCWV) is a key atmospheric variable and its evaluation is generally performed, at global scale, through the use of satellite data. Recently a new algorithm, called AIRWAVE (Advanced Infra-Red Water Vapour Estimator), has been developed for the retrieval of the TCWV from the Along-Track Scanning Radiometer (ATSR) instrument series. The AIRWAVE algorithm performs the TCWV retrieval exploiting the dual view of the ATSR instruments using the infra-red channels at 10.8 and 12 μm and combining nadir and forward observation geometries. The algorithm was used to produce a TCWV database from the whole ATSR mission. When compared to independent TCWV products, AIRWAVE Version 1 (V1) database shows very good agreement with almost no bias all over the ATSR missions, with the exception of the polar and the costal region where AIRWAVE underestimate the TCWV amount. In this paper we describe an updated version of the algorithm, specifically developed to overcome these problems. The AIRWAVE Version 2 (V2) accounts for the atmospheric variability at different latitudes and the associated seasonality. In addition, the dependency of the retrieval parameters on satellite across-track viewing angles is now explicitly handled. With the new algorithm we produced a second version of the AIRWAVE dataset. As for V1, the quality of V2 dataset is assessed through the comparison with the Special Sensor Microwave/Imager (SSM/I) and with the Analyzed Radiosounding Archive (ARSA) TCWV data. Results show significant improvements in both biases and RMSE, especially in polar and costal regions. A qualitative and quantitative estimate of the main error sources affecting the V2 TCWV dataset is also given. The new dataset has also been used to estimate the water vapour climatology from the 1991-2012 time series.

1 Introduction

A key issue in assessing the climate change is the precise knowledge of the distribution and variability of the Total Column of Water Vapour (TCWV), i.e. the vertically integrated atmospheric water vapour content. Actually, the TCWV is closely linked to clouds, precipitation and thus to the hydrological cycle (Allan et al., 2014) and for this reason it is one of the GCOS (Global

Atmos. Meas. Tech. Discuss., https://doi.org/10.5194/amt-2018-186
Manuscript under review for journal Atmos. Meas. Tech.
Discussion started: 20 June 2018

Atmospheric Measurement Techniques Discussions

Climate Observing System) Essential Climate Variables (ECVs). Since water vapour plays such a crucial role in meteorological as well as in climatological aspects, it is important to gather spatial and temporal thorough information about its distribution. At global scale, this can be achieved through the use of satellite missions. In the last decades measurements from several sensors were used for this purpose. Among them, sensors operating in the microwave regions as the Special Sensor Microwave Imager (SSMI onboard Defense Meteorological Satellite Program (DMSP) satellites) are used to infer accurate TCWV amount over ocean surfaces (Wentz, 1997), while sensors operating in the visible and near-infrared spectral range provide precise TCWV retrieval on land surfaces (e.g. Medium Resolution Imaging Spectrometer (MERIS)/ENVISAT (Lindstrot et al., 2012), or Moderate Resolution Imaging Spectroradiometer (MODIS) on the Terra and Aqua satellites (Diedrich et al., 2015)). The Along-Track Scanning Radiometer (ATSR, Delderfield et al. (1986)) instrument series had as main objective the accurate retrieval of sea surface temperature for climate studies. However, Casadio et al. (2016) demonstrated that it is possible to retrieve accurate and precise TCWV from its day and night time measurements, combining the ATSR Brightness Temperature (BT) collected from nadir and forward views in the channels at 10.8 and 12 μm in clear sky day and night sea scenes. The algorithm (named AIRWAVE, Advanced Infra-Red Water Vapour Estimator) exploits a sea emissivity dataset and calculations performed with a dedicated Radiative Transfer Model (RTM). A detailed description of the AIRWAVE algorithm is given in (Casadio et al., 2016). The first version of AIRWAVE TCWV dataset (hereafter V1), spanning from 1991 to 2012, is freely available from the GEWEX G-VAP website (G-VAP website) in form of monthly fields at $2^\circ \times 2^\circ$ regular grid resolution (Schroder et al., 2018). It's worth underlying here that V1 was developed to demonstrate the possibility of retrieving TCWV values from the ATSR measurements. The main goal pursued in its development was to have a simple software that could produce good results when compared to independent datasets. For this reason, in the V1 algorithm several approximations were made.

Papandrea et al. (2018), aiming at the validation of the AIRWAVE-v1 dataset, compared the data with the TCWV from SSMI and Analyzed Radiosounding Archive, (ARSA website)) for the whole mission. This exercise demonstrated a general good quality of AIRWAVE-v1 dataset apart for the polar regions and some coastal regions where an underestimation of the TCWV was found. In this paper we describe the new version of the AIRWAVE algorithm (hereafter V2) developed to overcome theese weaknesses by accounting for latitudinal and angular variations of the retrieval parameters. The new algorithm has been applied to all the available ATSR Level 1B Top of Atmosphere radiance products acquired over water surfaces in clear sky and in day/night conditions (same as for V1) to produce the V2 dataset. We show here the new TCWV climatologies derived from the 20 years of ATSR data together with the results of an extensive validation exercise performed repeating the same comparisons reported in (Papandrea et al., 2018). The new dataset shows improvements in terms of both bias and spread with respect to what achieved with V1.

This article is structured as follows: In section 2 we describe the new algorithm developed to produce V2, the improvements in retrieval scenarios and the strategy used for the selection of latitude and seasonal dependent retrieval parameters. In section 3 we describe the V2 dataset, the TCWV climatology and its validation agains SSMI and ARSA data and compare the performances of V2 against V1, finally, conclusions are given in section 4.

Atmos. Meas. Tech. Discuss., https://doi.org/10.5194/amt-2018-186
Manuscript under review for journal Atmos. Meas. Tech.
Discussion started: 20 June 2018

Atmospheric Measurement Techniques Discussions

2 The AIRWAVE version 2

Papandrea et al. (2018) demonstrated the general high quality of AIRWAVE-v1 by comparing the retrieved TCWV with corresponding SSMI and ARSA TCWV. However, in the same paper, the authors highlighted that at latitudes higher than 50° the agreement was not as good as for the rest of the globe. They speculated that this was due to the fact that AIRWAVEv1 makes use of average retrieval parameters, calculated under tropical and mid-latitude atmospheric scenarios. This choice was driven by the consideration that, being V1 applicable to water and cloud-free scenes only, the number of cloud-free measurements over the sea at high latitudes is significantly smaller than at mid-latitudes and tropical regions. Thus, a trade-off between generality (i.e. good precision at all latitudes), actual latitudinal coverage of cloud-free measurements and software complexity was the main driver for this choice. Moreover, V1 makes use of retrieval parameters computed for the along track viewing geometries only and uses an a-posteriori correction for the scenes pointing outside the orbit track.

The need to have a TCWV dataset of homogeneous quality at all latitudes and viewing geometries has driven the development of an improved version of the AIRWAVE algorithm, V2. The improvements were achieved through three main steps. Firstly, we modified the way in which some of the approximations of the solving equations were handled, leading to an improved retrieval precision. Secondly, we computed the retrieval parameters taking into account both their seasonal and latitudinal dependence. Finally, we calculated the retrieval parameters for different viewing angles to directly account for across track variations. We discuss these modifications in the following subsections. All the computations described in the paper have been made using the HITRAN2008 database (Rothman et al., 2009) for the spectroscopic data and the IG2 database (Remedios et al., 2007) version 4.1 for the atmospheric scenarios. We recall here that the IG2 database was developed to be used as model atmosphere in the analysis of the Michelson Interferometer for Passive Atmospheric Sounding (MIPAS)/ENVISAT measurements (that cover the same spectral region of the IR channels of ATSR). The IG2 database contains atmospheric vertical profiles of pressure, temperature and abundances of the molecules active in the the MIPAS spectral region, different for each year of the mission and divided into six latitudinal bands (polar, mid-latitude and equatorial for both north and south hemispheres) and four seasons.

2.1 Improvements in the solving equations

The starting point for the calculations of V2 retrieval parameters is the master equation of AIRWAVE Version 1. Since the expressions are the same for both nadir and forward geometry, we report here the equations for the general case, omitting the subscripts NAD (for NADIR) of FWD (for FORWARD) geometries. We reproduce here some of the equations reported in (Casadio et al., 2016) to help the reader in the comprehension of this article. The master equation of AIRWAVE algorithm is eq. (12) of the above mentioned work (now eq. 1):

$$\ln \frac{J_1^{\lambda_1}}{J_2^{\lambda_2}} = \ln \frac{F_1^{\lambda_1}}{F_2^{\lambda_2}} + \ln \frac{\epsilon_1^{\lambda_1}}{\epsilon_2^{\lambda_2}} + \ln \frac{\gamma_1^{\lambda_1}}{\gamma_2^{\lambda_2}} + \lambda_2 \tau_2 - \lambda_1 \tau_1 \quad (1)$$

where J_1 is the radiance that reaches the TOA for the 10.8 μm channel (λ_1), J_2 is the radiance that reaches the TOA for the 12 μm channel (λ_2), F includes the atmospheric and surface radiance contribution, ϵ is the sea emissivity, γ is a constant

Atmos. Meas. Tech. Discuss., https://doi.org/10.5194/amt-2018-186
Manuscript under review for journal Atmos. Meas. Tech.
Discussion started: 20 June 2018

Atmospheric Measurement Techniques Discussions

arising from the Planck law, τ are the optical depths at the two wavelength. Since only H_2O and CO_2 significantly affect the optical depth into ATSR Thermal Infrared (TIR) channels we can write:

$$\ln\frac{J_1^{\lambda_1}}{J_2^{\lambda_2}} = \ln\frac{F_1^{\lambda_1}}{F_2^{\lambda_2}} + \ln\frac{\epsilon_1^{\lambda_1}}{\epsilon_2^{\lambda_2}} + \ln\frac{\gamma_1^{\lambda_1}}{\gamma_2^{\lambda_2}} + \lambda_2\tau_2^{H_2O} - \lambda_1\tau_1^{H_2O} + \lambda_2\tau_2^{CO_2} - \lambda_1\tau_1^{CO_2} \tag{2}$$

then re-naming

$$G = \ln\frac{F_1^{\lambda_1}}{F_2^{\lambda_2}}, E = \ln\frac{\epsilon_1^{\lambda_1}}{\epsilon_2^{\lambda_2}}, \chi = \ln\frac{\gamma_1^{\lambda_1}}{\gamma_2^{\lambda_2}} \tag{3}$$

we get:

$$\ln\frac{J_1^{\lambda_1}}{J_2^{\lambda_2}} = G + E + \chi + \lambda_2\tau_2^{H_2O} - \lambda_1\tau_1^{H_2O} + \lambda_2\tau_2^{CO_2} - \lambda_1\tau_1^{CO_2} \tag{4}$$

In V1 we assume that the optical depth (τ) is the product of the vertical column of H_2O by the relative effective absorption cross section (σ), normalised to the air mass factor (AMF) for the given line of sight angle:

$$\lambda_2\tau_2^{H_2O} - \lambda_1\tau_1^{H_2O} = \frac{\lambda_2\sigma_2 - \lambda_1\sigma_1}{AMF}TCWV \tag{5}$$

This implies that a linear behaviour exists between the water vapour optical depth and the TCWV is envisaged. The linear dependence allows to solve the AIRWAVE equation and to retrieve TCWV with good accuracy.

In the development of AIRWAVEv2 we investigated the possibility to find a more accurate solution of the AIRWAVE equation still preserving the linear dependence between water vapour optical depth and TCWV. We recall here that in AIRWAVEv1 the water absorption cross sections were obtained using MODTRAN (Berk et al., 2008) while all the other values were obtained with the dedicated RTM, developed for ATSR measurements simulations and described in (Casadio et al., 2016). For V2, a different approach was adopted for the calculation of effective absorption cross section. We have simulated ATSR synthetic radiances for the different atmospheric scenarios of the IG2 database and thus with different water vapor content. A detailed descriptions of these simulations is given in Sect. 2.2.

Using these simulations and ATSR-SSMI collocated TCWV, we verified that $ln\frac{J_1^{\lambda_1}}{J_2^{\lambda_2}}$ correctly reproduces the real measurement behaviour as function of TCWV and that this relation is in first approximation linear. Therefore we can now re-write equation (4), isolating the terms that account for the water content ($\tau_1^{H_2O}$and $\tau_2^{H_2O}$):

$$\ln\frac{J_1^{\lambda_1}}{J_2^{\lambda_2}} - G - \chi - E - \lambda_2\tau_2^{CO_2} + \lambda_1\tau_1^{CO_2} = \lambda_2\tau_2^{H_2O} - \lambda_1\tau_1^{H_2O} = \Delta\tau \tag{6}$$

Atmos. Meas. Tech. Discuss., https://doi.org/10.5194/amt-2018-186
Manuscript under review for journal Atmos. Meas. Tech.
Discussion started: 20 June 2018

Atmospheric Measurement Techniques Discussions

The G term of equations (3) and (4) is not as constant as supposed and partially verified in (Casadio et al., 2016), and may depend on the different water vapor content. For this reason, for each atmospheric scenario the average of all the G values obtained with different water vapour content is used. Equation (6) can thus be written as:

$$\ln \frac{J_1^{\lambda_1}}{J_2^{\lambda_2}} - G_{AVG} - \chi - E - \lambda_2 \tau_2^{CO_2} + \lambda_1 \tau_1^{CO_2} = \Delta\tau \tag{7}$$

Therefore for each scenario and geometry we can write:

$$\ln \frac{J_1^{\lambda_1}}{J_2^{\lambda_2}} - G_{AVG} - \chi - E - \lambda_2 \tau_2^{CO_2} + \lambda_1 \tau_1^{CO_2} = \Delta\tau = \Delta\sigma \cdot TCWV + \Delta\rho \tag{8}$$

In this equation, $\Delta\sigma$ and $\Delta\rho$ represent the slope and intercept of the straight line representing the behaviour of the term containing the radiances as a function of the TCWV. In the testing version of the V2 code, we estimated these parameters using the values of the radiances and the TCWV obtained perturbing the IG2 water vapor amount by a factor 0.5 and 1.5. With respect to V1, in V2 the $\Delta\sigma$ is a sort of "effective" water vapour cross section. Grouping the terms in equation (8) as in (Casadio et al., 2016) we get:

$$TCWV = \Phi - \frac{G}{\Delta\sigma} \tag{9}$$

where Φ is the "water vapor pseudo-column" that in V2 is defined as :

$$\Phi = \frac{\ln \frac{J_1^{\lambda_1}}{J_2^{\lambda_2}} - \chi - E - \lambda_2 \tau_2^{CO_2} + \lambda_1 \tau_1^{CO_2} - \Delta\rho}{\Delta\sigma} \tag{10}$$

This formula is sightly different from the one used in (Casadio et al., 2016) due to the presence of the $\Delta\rho$ term:

$$\Phi = \frac{\ln \frac{J_1^{\lambda_1}}{J_2^{\lambda_2}} - \chi - E - \lambda_2 \tau_2^{CO_2} + \lambda_1 \tau_1^{CO_2}}{\Delta\sigma} \tag{11}$$

If in eq. 9 now we explicit the dependence on the viewing angles we get:

$$TCWV_{NAD} = \Phi_{NAD} - \frac{G_{NAD}}{\Delta\sigma_{NAD}} \quad and \quad TCWV_{FWD} = \Phi_{FWD} - \frac{G_{FWD}}{\Delta\sigma_{FWD}} \tag{12}$$

while the TCWV given by the combined use of nadir and forward pseudo column is:

$$TCWV = \alpha \cdot \Phi_{NAD} + \beta \cdot \Phi_{FWD} \tag{13}$$

where

$$\alpha = \frac{1}{1 - \frac{\Delta\sigma_{FWD}}{\delta \cdot \Delta\sigma_{NAD}}} \quad and \quad \beta = \frac{1}{1 - \frac{\delta \cdot \Delta\sigma_{NAD}}{\Delta\sigma_{FWD}}} \quad with \quad \delta \approx \frac{G_{FWD}}{G_{NAD}} \tag{14}$$

Atmos. Meas. Tech. Discuss., https://doi.org/10.5194/amt-2018-186
Manuscript under review for journal Atmos. Meas. Tech.
Discussion started: 20 June 2018

Equations (10), (12) and (13) are the solving equations used in V2, while V1 makes use of equations (11), (12) and (13). The new equations were used to compute a new set of retrieval parameters. For consistency purposes, in V2 the computations were performed with the dedicated RTM as for V1. An example of the difference between the parameters used for V1 and V2 is given in Table 1 for tropical scenario and sub-satellite view configuration. As can be noticed, the larger differences are for α, β and $\Delta\sigma$ parameters: there is a reduction of the α and β parameters of a factor of about 50 from v1 to v2, while $\Delta\sigma$ is reduced by a factor of 30.

These changes have a direct effect on the retrieval precision. We can have an estimate of the improvements of the precision of V2 retrievals against V1 using the following consideration: in AIRWAVE we can estimate the expected precision by multiplying the measurement random error by a factor of $\alpha/\Delta\sigma$. Therefore in V1 we multiply the random error by a factor of 53/1.9 (= 28) while in V2 the multiplicative factor is 1.7/0.08 (= 21). In case of polar atmosphere this ratio is further reduced reaching a value of 13. Since the overall random error is about 0.25% for AATSR and ATSR-2 and 0.6% for ATSR-1, we have that the precision for AATSR and ATSR-2 improves from 7% to 5% and for ATRS-1 goes from 17% to 12% for tropical atmosphere and in V2 reaches 3% for AATSR ad ATSR-2 and 8 % for ATSR-1 in polar atmosphere. From these considerations it follows that V2 parameters should improve the retrieval performances.

2.2 Improvements in the retrieval scenario

In V1 we make use of the same set of retrieval parameters for all measurements of a single ATSR instrument. Independent sets of parameters are calculated for the three missions, while within each mission no dependencies on different atmospheric/surface conditions or seasons was considered. In V2 the retrieval parameters are estimated not only according to the instrument type but also accounting for possible latitudinal and seasonal variations. To this aim, we have used the aforementioned RTM to compute all the required quantities exploiting the model atmospheres of the IG2 database. Since the IG2 database was specifically developed for the MIPAS/ENVISAT mission, it covers only the time range from 2002 to 2012, while the ATSR series operated from 1991 to 2012. However, the inter-annual variations of most of the species active in the ATSR thermal infrared spectral range are generally much smaller than the corresponding seasonal ones. Therefore we used the data for one year only, and we considered the inter-annual variations as systematic error sources (see Appendix A for an estimate of these errors).

To better reproduce the variability of the atmospheric scenarios that were observed by the ATSR instruments, we therefore calculated the retrieval parameters exploiting the profiles for all the six latitude bands and the four seasons included in the IG2 datasets for one year only.

The AIRWAVE solving equations do not explicitly make use of the Sea Surface Temperature (SST). However, it is used in the Radiative Transfer (RT) computations to estimate the retrieval parameters. The sea surface emissivity values are instead used both in the parameters estimation and in the AIRWAVE retrieval. While over land the emissivity is characterised by a large spatial difference (it indeed varies as a function of soil type, vegetation cover, etc.), over sea its variation is in general relatively small. For this reason in V1 we used constant emissivity values calculated for the nadir and forward viewing angles with fixed SST (285K) and wind speed (3 m/s). In the new version of the algorithm, coherently with the approach used for the atmospheric scenarios, the retrieval parameters have been computed using dedicated SST values for each season and latitude

band. The SST monthly means were produced for the corresponding six latitude bands and for the four seasons using ECMWF ERA-Interim daily fields data with a regular latitude/longitude grid of 0.75° × 0.75° (241 × 480 grid points).

The emissivity of each scenario has been computed using the data extracted from the University of Edinburgh database (Embury et al., 2008). This dataset contains emissivities tabulated as a function of wave number (600-3350 cm^{-1} or 3-16.7 μm), viewing angle (0-85°), temperature (270-310 K), and wind speed (0-25 m/s at 12.5 m). For the RTM computations we used the full spectral dependency of the emissivity. Since in equation 3 of AIRWAVE we use a single emissivity value for each channel, we estimated it by convolving the spectral emissivity with the ATSR filter functions. The nadir and forward viewing angles of the instruments have been defined at eleven tie points of the ATSR swath (pixels associated with specific points equally spaced across a single image or instrument scan). For each tie point we then used the corresponding viewing angles to extract the correct emissivity values, with a fixed wind speed (3 m/s), as for V1.

2.3 Across track variations of the retrieval parameters

A simplification present in V1 is that the retrieval parameters are calculated only for the sub-satellite viewing angles (55° for forward view and 0° as nadir viewing angle). However, due to the ATSR configuration, the nadir viewing angles varies from 0° (sub-satellite) to approximately 21° (across track edge of the ATSR swath, ± 250 km from nadir), while the forward viewing angles range from 53° to 55°. Significant TCWV differences between centre and edge swath are, thus, expected.

In V1 the across-track dependence of TCWV is corrected a-posteriori. The correction was calculated on the basis of TCWV retrievals performed over simulated brightness temperatures (BTs).

However, this approximation might not be sufficiently adequate depending on the used atmospheric scenario. Furthermore, a slight asymmetry with respect to the sub-satellite track position is expected as the ATSR instruments are tilted of about 4° respect to the flying direction of the satellite. Therefore the a-posteriori correction of V1 cannot fully reproduce all these features. In V2 we replaced the a-posteriori correction by directly calculating the retrieval parameters for each of the above described tie points of the nadir and forward swaths and interpolating the results at each position of the ground pixels.

2.4 Selection of the retrieval parameters

The computation of the retrieval parameters, described in the previous sections, produced a set of 1584 retrieval parameters for each ATSR mission (6 coefficients × 6 latitude bands × 4 seasons × 11 tie points) store in dedicated look-up tables (LUTs). In order to select the most suitable set of parameters for each ATSR measurement, a multivariate interpolation on a 3-dimensional grid (trilinear) has been applied to the six retrieval coefficients ($\Delta\sigma$, G, $\Delta\rho$) and the emissivity for both the FWD and the NAD geometries.

3 AIRWAVE V2 dataset: description, climatology and validation

The AIRWAVE V2 TCWV data are produced, as for the V1 dataset, processing Level 1B measurements acquired over water and in clear sky conditions in both nadir and forward views (according to the Level 1B cloud mask). The output files are saved

195 in Interactive Data Language (IDL) binary files (.sav extension), however they can be easily converted in other formats (e.g. netcdf) upon request. The parameters contained into the files are structured in two groups, in the first one (named HIRES) the parameters are given at native resolution (1×1 km^2) while in the second one (named SSMI) the parameters have been aggregated to SSMI resolution ($0.25^\circ \times 0.25^\circ$ grid). Both groups contain: the TCWV, the latitude, the longitude, the across track index value (0-512) and a day/night flag. The SSMI group, in addition, contains the value of the standard deviation and
200 the number of elements aggregated within the SSMI grid cell.

The climatologies have been derived using all the available years and sensors of the ATSR family. Using the AIRWAVEv2 products aggregated at the $0.25^\circ \times 0.25^\circ$ grid, we obtained for each month day/night TCWV averages and standard deviations. The final monthly files are also saved as IDL binary files but can be converted in other formats and are available upon request.

Figures from 1 to 4 show sketches of the climatology for January, April, July and October obtained from 20 years of ATSR
205 daytime measurements. Similar results are obtained for nigh-time retrievals (not shown here). In each figure we report on the left the TCWV global distribution at 0.25° grid resolution and its standard deviation on the left panel, in the central panel on top row we show the TCWV meridional mean together with its standard deviation, while on the bottom row we report the TCWV zonal mean.

The geographical distribution of the median values of the TCWV reflects the behaviour of general atmospheric circulation.
210 Higher TCWV values, associated to strong convection in the Inter Tropical Convergence Zone (ITCZ), are located around the equator while lower values are found in the polar regions. Also the zonal means as a function of latitudes reflect this behaviour, while the zonal meridional means show a more homogeneous behaviour. Here lower TCWV values are found in coincidence of longitudes where we have extended land presence in the equatorial region. The mean and the absolute standard deviation show similar features, with higher values in the ITCZ region. As can be noticed, the seasonal movements of the ITCZ from North
215 (in Northern hemisphere summer) to South (in Northern hemisphere winter) can be clearly detected (Castelli et al., 2018). In general, the standard deviations in the region where the TCWV maximum is located are of the order of 15% and up to 20% in polar regions. The zonal means reflect the shift of the ITCZ during the year with maximum values of TCWV in northern hemisphere reached in July.

The quality of the V2 dataset is evaluated through the same method adopted for V1 and reported in (Papandrea et al., 2018).
220 The V2 dataset is compared to the TCWV obtained from the SSMI satellite and to data available from the ARSA.

In this contest, these two datasets are complementary, as the SSMI TCWV are not retrieved for measurements in proximity of coasts (minimum distance about 60 km), while the selected ARSA stations are located in coastal areas.

The SSMI dataset is produced from the SSMI instrument series onboard the Defense Meteorological Satellite Program (DMSP) polar orbit satellites since 1987. For this comparison, we used the 0.25° v7 daily product obtained from the F13
225 satellite. In fact, differently from the other DMSP satellites, the local time of the ascending node of F13 (18:00 UTC) is more stable than the one of the other satellites with only a variation of 1 hour during the whole mission. For the comparison with SSMI we used the AIRWAVE V2 data aggregated at 0.25° resolution covering the time period from 1995 to 2009. The ARSA dataset spans from January 1979 to present and contains water vapour concentration profiles at specific pressure levels. To obtain the TCWV we vertically integrate these values. For the comparison with the ATSR data, only stations surrounded, even

Atmos. Meas. Tech. Discuss., https://doi.org/10.5194/amt-2018-186
Manuscript under review for journal Atmos. Meas. Tech.
Discussion started: 20 June 2018

partially, by water are used. More details about the selection of ATSR and ARSA coincident data are reported in (Papandrea et al., 2018).

In Fig. 5 we show the Bi-dimensional histograms of the comparisons between V2 and SSMI (left panel) and ARSA (right panel). The SSMI measurements are homogeneously distributed over the globe, while ARSA radiosounding stations are mainly located at mid-latitudes (see Fig.7) and this is reflected in the bulk of the ARSA TCWV values ranging between 0-30 kg/m^2.

Globally, a good correlation is obtained against both datasets, as highlighted by the correlations and bias values reported in the same figure. In particular the comparison with the same histograms of V1 (see Fig. 1 of Papandrea et al. (2018)) highlights the correction of negative values in polar and costal regions in the new version of the dataset.

The zonal means (calculated in bins of 2 degrees for all the datasets, and reported in Fig. 6) also show the good quality of V2 data with respect to both radiosoundes and satellite data at all latitudes. In Fig. 6, the V1 data are overplotted for comparison. The improvement in the performances of the new dataset is clearly visible at all latitudes. Figure 7 reports the geographical distribution of the mean TCWV differences with respect to SSMI and ARSA in absolute and percentage values. In comparison to AIRWAVE-v1, see Fig. 3 of Papandrea et al. (2018), the differences with SSMI are reduced at all latitudes. The longitudinal patterns of the differences are similar to the ones of V1 except for the equatorial pacific region where V2 shows a slightly higher positive bias. The reasons for this behaviour are under investigation. In the majority of costal regions, where V1 underestimated the TCWV, V2 is now in agreement with ARSA results (no SSMI data close to coast).

In Table 2 we summarise the results of this comparison for both ARSA and SSMI and for different scenarios and missions. The average bias is about 0.0 $\pm$ 4.7 kg/m^2 with respect to SSMI and 0.2 $\pm$ 6.1 kg/m^2 with respect to ARSA. If we compare these results with the ones for V1 we can clearly see the improvement in both the biases and the standard deviations(0.7 $\pm$ 5.7 kg/m^2 with respect to SSMI and 0.8 $\pm$ 7.7 kg/m^2 with respect to ARSA). As can be seen from Fig.s 6 and 8 and from results in Table 2 (to be compared with those in Table 2 of Papandrea et al. (2018)) the improvement in the bias is obtained at all latitudes; it is however more evident in polar regions (from 5.5 $\pm$ 5.1 kg/m^2 in V1 to 1.3 $\pm$ 3.5 kg/m^2 in V2 versus SSMI and from 4.1 $\pm$ 6.5 kg/m^2 in V1 to 0.9 $\pm$ 4.6 kg/m^2 in V2 when using ARSA). Slight difference between the three ATSR missions are consistent with the related uncertainties.

In Fig. 8 we show monthly mean evolution of the differences (and their standard deviation), between the TCWV obtained from correlative measurements and V2. As for V1, these differences are quite stable over time, with the exception of the beginning of the ATSR-1 mission (1991-1994). As explained in Papandrea et al. (2018), this can be due to the failure of 3.7 μm channel that impacted the ATSR cloud screening. In general, the differences with respect to the radiosonde exhibit a higher seasonality due to pronounced variability of atmospheric and surface conditions in costal areas.

It is worth noticing that the spread of the AIRWAVE-v2 is always smaller than the one of AIRWAVE-v1. This is partially due to the new algorithm that reduces the random error component due to noise on the retrieved TCWV.

The above described results indicate that the V2 algorithm reduces the global bias with respect to SSMI, from about 0.7 kg/m^2 of AIRWAVE-v1 to 0.0 kg/m^2 and improves the standard deviations (STD) of up to 20% with respect to V1. In V2, the STD values are essentially constant for all the scenarios and missions, highlighting the un-biased nature of the dataset with

respect to SSMI (cloud-free). When using ARSA data the bias reduces from 0.8 kg/m^2 to 0.2 kg/m^2 and the standard deviations of 21%.

4 Discussion and Conclusions

The second version of the AIRWAVE TCWV dataset described in this work, has been validated against ARSA and SSMI equivalent products.

As expected also from the analysis of synthetic retrievals, the most significant AIRWAVE Version 2 improvement is achieved at polar latitudes. However, improvements at mid-latitudes are also found. These improvements are due to the fact that the V2 retrieval parameters account for atmospheric variability. No statistically significant trend can be found in the comparison with SSMI and ARSA in both versions of the database, while a seasonal dependence of the differences is observed, with larger bias in July and August, mainly due to the differences in mid-latitude north TCWV retrievals. In general, we find slightly drier results with respect to ARSA and SSMI with both versions. This is possibly due to the fact that the temporal mismatch between the ATSR and the correlative measurements does not allow to exclude all SSMI TCWV retrieval obtained under cloudy conditions, or to wrong cloud mask assignation. As discussed, the use of retrieval parameters that are calculated in conditions different from the ones present in the observed scenario can cause biases on the obtained TCWV. We point out that the major source of errors on the retrieved TCWV comes from the temperature profile assumptions, while erroneous assumptions of other gases (e.g. HNO_3, CFC-11, CFC-12, CO_2) have an almost negligible impact. The obtained RMSE value of about 7% is of the same order of this error.

Beside the improvements on ATSR TCWV retrievals given by the AIRWAVE Version 2 dataset, the method described in this work can be the basis for a similar approach for SLSTR (Sea and Land Surface Temperature Radiometer, on board COPERNICUS SENTINEL-3, (Donlon et al., 2012)).

Acknowledgements

This work has been performed under the ESA-ESRIN Contract No. 4000108531/13/I-NB. The authors gratefully acknowledge ECMWF for SST data, the GlobVapour project for providing the combined MERIS+SSM/I water vapour product. SSM/I and SSMIS data are produced by Remote Sensing Systems. Data are available at www.remss.com/missions/ssmi.

5 Appendix A: Evaluation of AIRWAVE Version 2 main systematic and random errors

This appendix provides an estimate of the main error sources (random and systematic) that affect the V2 dataset. To facilitate the use of the errors together with the TCWV contained into the dataset, we summarize the results of this appendix in Table 3. V2 retrieval parameters accounts for atmospheric and surface variability of the observed scenes. However, real observed scenes can obviously deviate from the simulated ones. An evaluation of the errors induced by these deviations is then required. For this reason we analyse, through the use of synthetic radiances, the major sources of errors that can affect AIRWAVEv2 retrieval i.e.

Atmos. Meas. Tech. Discuss., https://doi.org/10.5194/amt-2018-186
Manuscript under review for journal Atmos. Meas. Tech.
Discussion started: 20 June 2018

(in order of importance): the influence of the atmospheric temperature profile variations, the impact of sea emissivity changes due to the wind and the impact of interfering atmospheric species. Furthermore, an estimate of the random error component due to the noise is also reported.

5.1 Retrieval approximations

In order to evaluate the impact of systematic errors due to the retrieval approximations, we performed some tests of TCWV retrievals from simulated radiances. We used Top Of the Atmosphere (TOA) sub-satellite track Brightness Temperatures (BTs) simulated with the RTM at 10.8 and 12 μm in nadir and forward geometries as input to the retrieval chain (no random noise was added). The BTs were produced using different TCWV amounts for each given scenario (e.g. water vapour profiles were multiplied by 0.5, 0.75, 1.25, 1.5), while all the other atmospheric profiles were kept constant. Results of this exercise show that TCWV is correctly retrieved with an error of $\pm$ 3%. For comparison purposes, we performed a similar test using the V1 approach. For V2 tests, the same atmospheric conditions used to compute the retrieval parameters have been adopted, while for V1 larger errors are expected due to the fact that the atmospheric variability is not taken into account. Despite this, this analysis shows that V1 performs well for medium-high TCWV (>30 kg/m^2), where the differences are below 10%. For TCWV values between 10-20 kg/m^2, the differences range between -10 and -30%. V1 underestimates the low TCWV values (below 10 kg/m^2) with differences going from -50% to -150/-200%. This was also reported in (Casadio et al., 2016), where the authors compared AIRWAVE TCWV with collocated ECMWF counterparts showing a dry bias at high latitudes (where the TCWV values are small). The tests on synthetic radiances indicate that the V2 parametrisation solves this issue.

5.2 Atmospheric temperature profiles

One of the main error sources that can affect the AIRWAVE TCWV retrieval is the assumption of a fixed temperature profile. Actually, the atmospheric opacity is closely linked to the atmospheric density and thus to the atmospheric temperature. To estimate the impact of temperature on the retrieved TCWV, twenty different temperature profiles were randomly perturbed by $\pm$3 K on a 1 km equi-spaced altitude grid. Then, simulated BTs were produced with the RTM and were used to perform the TCWV retrievals for the three instruments in equatorial, mid-latitude and polar July conditions for the north hemisphere. and the results were compared with respect to the unperturbed case. In the third column of Table 3 we summarise the findings of this analysis for each of the three instruments, reporting the STD of the difference both in absolute and in percentage values.

The impact of the perturbations on the temperature profile is of the order of 6% and is higher in the equatorial and mid-latitude regions and lower at the poles. Indeed, in the equatorial region, due to the higher water vapour content, the atmosphere is more opaque than at the poles so that temperature variations have a larger impact on the retrieved TCWV.

5.3 Wind Speed

A further source of error that can affect the TCWV retrievals is the value used for the sea emissivity, which enter directly into equations (10) and (11). Sea emissivity depends upon wavelenght, sea surface temperature, viewing angles and wind speed.

As stated in Sect. 2.2, in V2 we accounted for emissivity variations due to the viewing angles and sea surface temperatures. All the calculations were performed at a fixed wind value of 3 m/s. In order to assess the possible systematic effects due to wind variations on the retrieved values, we varied the emissivity according to the wind speed at three values as tabulated in the University of Edinburgh emissivity database: 1 m/s, 10 m/s and 25 m/s.

The emissivity has a different value and spectral behaviour with different wind speeds. The fourth column of Table 3 report the difference of the TCWV retrieved for simulated measurements with the 25 m/s wind speed with respect to the reference case. As expected, the impact is almost negligible in the equatorial band, where the higher opacity of the atmosphere reduces the sensitivity of ATSR measurements to the surface conditions, while increases toward the poles where, due to the low atmospheric opacity, the surface effects become relevant with respect to the atmospheric component. Furthermore, in case of polar conditions, the effects of the wind on the retrieved TCWV is not linear, with enhanced variations for wind speed of 25 m/s, as not only the intensity but also the spectral shape of the surface emissivity varies in function of the wind speed. The possible presence of white caps, generated by high speed winds, has not been considered in this study

5.4 Interfering atmospheric constituents

The AIRWAVE algorithm, in both versions, accounts for the contribution to the radiance of the two main gases active into the ATSR channels (H_2O and CO_2). However some other species have spectroscopic features in the ATSR channels. In Fig. 9, the CO_2, HNO_3 and CFCs spectra in the 10-13 μm wavelength range are shown, along with the ATSR filter functions (all in arbitrary units). In order to have a complete view of the possible error components, we assessed the interfering species impact in case their abundance differs from the one used in the reference scenarios to compute the retrieval parameters.

Among the considered species, HNO_3 shows significant latitudinal and seasonal variability while CO_2 and CFCs exhibit inter-annual trends (Remedios et al., 2007). For this reason we separately accounted for the effects due to latitudinal and inter-annual variability. We used the IG2 database version 4.1 and our RTM to produce synthetic BTs. For each season/latitude band we generated synthetic BTs using the proper IG2 atmospheric status but the profile of the investigated species, for which we used all the different available profiles. The generated BTs were then used to retrieve the TCWV to assess the systematic error induced by the expected variability of the interfering species.

Latitudinal and seasonal variations of HNO_3 impact ATSR-1 and ATSR-2 BTs more than AATSR, because of the different shapes of the TIR filter functions, and can produce differences up to 0.3 K in the 11 μm band (mid-latitude vs tropical north in January). For CFC-11 seasonal differences in the tropics are of the order of 0.001 K in the 12 μm band and for CFC-12 we get 0.03 K in the 11 μm band, while latitudinal variations reach 0.04 K from tropical to mid-latitude atmospheres for both channels. CO_2 latitudinal variations can produce a maximum difference of 0.003 K on nadir BT. The impact of maximum latitudinal variations of HNO_3, CFCs and CO_2 on the retrieved TCWV is reported in Table 3. The largest contribution is due to HNO_3 latitudinal variation and is of the order of 0.6%, while the CFCs latitudinal variations produce differences of 0.15% and CO2 of 0.01% only. Furthermore, the impact of using mid latitude profiles instead of tropical profiles for all species but H_2O has a maximum impact of 0.22%. Seasonal variations are almost negligible for CO_2 and CFCs, while they are only 0.6%

for HNO_3. Thus we can safely assume that the latitudinal and seasonal variations of the interfering species represent a minor error source for the AIRWAVE TCWV for both V1 and V2.

To evaluate the impact of inter-annual variations also for all the ATSR series, we would need the CO_2 and CFCs profiles from 1991 to 2012. However, as mentioned in the previous sections, the IG2 database contains data from the 2002 onwards. In this work, the CFCs and CO_2 profiles from 1991 to 2001 were inferred scaling the 2002 profiles using the trend given in the last IPCC report for CO_2 and in the Mauna Loa observatory website ((Global Monitoring Division website) website, see also Aoki et al. (2003) and Minschwaner et al. (2013)) for CFC-11 and CFC-12. The impact on the ATSR BTs due to the inter annual variations of CO_2 and CFCs has been evaluated for each mission. We calculated the synthetic spectra using the CFC-11, CFC-12 or CO_2 profile for the initial and final year of each mission. Then we calculated, for each instrument, the differences of retrieved TCWV at the beginning and at the end of each mission. Results for CO_2 and CFCs are shown in Table 3. The influence of CO_2 annual variations on the retrieved TCWV is of the order of 0.004 kg/m^2 (<0.01 %). For CFCs we obtain 0.002 kg/m^2. We can then conclude that the impact of VMR latitudinal and seasonal variations on retrieved TCWV is negligible (maximum value 0.6%), and that the systematic effect of CO_2 and CFCs long term variations over the missions are even smaller (0.07%).

5.5 Noise

Finally we analyse the impact of the measurement noise on the retrieved TCWV (see last column of Table 3). The measurement noise was simulated applying a random perturbation of $\pm$0.037 K on the BTs of the two channels of ATSR-2 and AATSR and a perturbation of $\pm$0.1 K on the ATSR-1 channels (Smith et al., 2012). For each instrument, we have generated one thousand values and we have evaluated the standard deviation of the obtained TCWV that we report in absolute and percentage values in Table 3. The standard deviation is maximum at the poles, as expected since there the TCWV and S/N ratio are lower. For V2 we get 18% for ATSR-1 and 6% for ATSR-2 and AATSR in the worst case. To be noticed that V2 approach has, for all the scenarios, better performances with respect of V1 (see Casadio et al. (2016)).

References

References

Allan, R. P., Liu, C., Zahn, M., Lavers, D., Koukouvagias, E., and Bodas-Salcedo, A.: Physically Consistent Responses of the Global Atmospheric Hydrological Cycle in Models and Observations, Surv. Geophys., 35, 533-552, doi:10.1007/s10712-012- 9213-z, 2014.

Aoki, S., Nakazawa, T., Machida, T., Sugawara, S., Morimoto, S., Hashida, G., Yamanouchi, T., Kawamura, K., and Honda,H.: Carbon dioxide variations in the stratosphere over Japan, Scandinavia and Antarctica, Tellus, 55B, 178-186, 2003.

ARSA website: http://ara.abct.lmd.polytechnique.fr/index.php?page=arsa, (accessed 17 March 2018).

Barton, I. J.: Global water vapor analyses over the oceans using along track scanning radiometer infrared data. Journal of Geophysical Research, 109, D02303. http://dx.doi.org/10.1029/2002JD002856, 2004.

Berk, A., Acharya, P. K., Bernstein, L. S., Anderson, G. P., Lewis, P., Chetwynd, J. H., and Hoke, M. L.: Band model method for modeling atmospheric propagation at arbitrarily fine spectral resolution. U.S. Patent n7433806, issued October 7, 2008.

Casadio, S., Castelli, E., Papandrea, E., Dinelli, B. M., Pisacane, G., and Bojkov, B.: Total column water vapour from along track scanning radiometer series using thermal infrared dual view ocean cloud free measurements: The Advanced Infra-Red WAter Vapour Estimator (AIRWAVE) algorithm. Remote Sensing of Environment 172,1-14, 2016.

Castelli, E., Papandrea, E., Valeri, M., Greco F. P., Ventrucci, M., Casadio, S., Dinelli, B. M.: ITCZ trend analysis via Geodesic P-spline smoothing of the AIRWAVE TCWV and cloud frequency datasets. Submitted to Atmospheric Research, 2018.

Delderfield, J., Llewellyn-Jones, D.T., Bernard, R., de Javel, Y., Williamson, E.J., Mason, I., Pick, D.R. and Barton, I.J.: The Along Track Scanning Radiometer (ATSR) for ERS-1. Proc. SPIE 589, 114-120, 1986.

Diedrich, H., Preusker, R., Lindstrot, R., and Fischer, J.: Retrieval of daytime total columnar water vapour from MODIS measurements over land surfaces. Atmos. Meas. Tech., 8, 823-836, 2015 www.atmos-meas-tech.net/8/823/2015/ doi:10.5194/amt-8-823-2015, 2015

Donlon, C., Berruti, B., Buongiorno, A., Ferreira, M.-H., Féménias, P., Frerick, J., Goryl, P., Klein, U., Laur, H., Mavrocordatos, C., Nieke, J., Rebhan, H., Seitz, B., Stroede, J., Sciarra, R.: The Global Monitoring for Environment and Security (GMES) Sentinel-3 mission, Remote Sensing of the Environment, 120, 27-57, http://dx.doi.org/10.1016/j.rse.2011.07.024, 2012.

Embury, O., Merchant, C., and Filipiak, M.: Refractive indices (500-3500 cm^{-1}) and emissivity (600-3350 cm^{-1}) of pure water and seawater, [Dataset]. http://dx.doi.org/10.7488/ds/162, 2008.

Global Monitoring Division website, http://www.esrl.noaa.gov/gmd/ccgg/trends/index.html#mlo_growth, (accessed 17 March 2018).

GEWEX G-VAP website, http://gewex-vap.org/, (accessed 17 March 2018).

Lindstrot, R., Stengel, M., Schröder, M., Schneider, N., Preusker, R., and Fischer, J.: Combined SSM/I and MERIS Water Vapour Products from the ESA GlobVapour project. In AGU Fall Meeting Abstracts (Vol. 1, p. 0217), December 2010.

Lindstrot, R., Preusker, R., Diedrich, H., Doppler, L., Bennartz, R., and Fischer, J.: 1D-Var retrieval of daytime total columnar water vapour from MERIS measurements, Atmos. Meas. Tech., 5, 631- 646, doi:10.5194/amt-5-631-2012, 2012.

Minschwaner, K., Hoffmann, L., Brown, A., Riese, M., Muller, R., and Bernath, P. F.: Stratospheric loss and atmospheric lifetimes of CFC-11 and CFC-12 derived from satellite observations, Atmos. Chem. Phys., 13, 4253-4263, 2013.

Papandrea, E., Casadio, S., De Grandis, E., Castelli, E., Dinelli, B.,M., Bojkov, B.: Validation of the Advanced Infra-Red Water Vapour Estimator (AIRWAVE) Total Column Water Vapour using Satellite and Radiosonde products. Annals of Geophysics, 61, Fast Track 8, doi: 10.4401/ag-7524, 2018.

Remedios, J. J., Leigh, R. J., Waterfall, A. M., Moore, D. P., Sembhi, H., Parkes, I., Greenhough, J., Chipperfield, M.P., and Hauglustaine, D.: MIPAS reference atmospheres and compar-isons to V4.61/V4.62 MIPAS level 2 geophysical data sets, Atmos. Chem. Phys. Discuss., 7, 9973–10017, doi:10.5194/acpd-7-9973-2007, 2007.

Rothman, L.S., Gordon, I. E., Barbe, A., Benner, D. Chris, Bernath, P. E., Birk, M., Boudon, V., Brown, L. R., Campargue, A., Champion, J. -P., Chance, K., Coudert, L. H., Dana, V., Devi, V. M., Fally, S., Flaud, J. -M., Gamache, R. R., Goldman, A., Jacquemart, D., Kleiner, I., Lacome, N., Lafferty, W. J., Mandin, J. -Y., Massie, S. T., Mikhailenko, S. N., Miller, C. E., Moazzen-Ahmadi, N., Naumenko, O. V., Nikitin, A. V., Orphal, J., Perevalov, V. I., Perrin, A., Predoi-Cross, A., Rinsland, C. P., Rotger, M., Simeckova, M., Smith, M. A. H., Sung, K., Tashkun, S. A., Tennyson, J., Toth, R. A., Vandaele, A. C., Vander Auwera, J.: The HITRAN 2008 molecular spectroscopic database, JQSRT, 110, 533-572, doi:10.1016/j.jqsrt.2009.02.013, 2009.

Schröder, M.: Product Validation Report Combined SSMI + MERIS, Issue 1 Revision 1, 21 August 2012.

Schröder, M., Lockhoff, M., Fell, F., Forsythe, J., Trent, T., Bennartz, R., Borbas, E., Bosilovich, M. G., Castelli, E., Hersbach, H., Kachi, M., Kobayashi, S., Kursinski, E. R., Loyola, D., Mears, C., Preusker, R., Rossow, W. B., and Saha, S.: The GEWEX Water Vapor Assessment archive of water vapour products from satellite observations and reanalyses, Earth Syst. Sci. Data, 10, 1093-1117, 2018 https://doi.org/10.5194/essd-10-1093-2018.

Smith, D., Mutlow, C., Delderfield, J.,Watkins, B., and Mason, G.: ATSR infrared radiometric calibration and in-orbit performance. Remote Sensing of Environment, 116, 4:16, 2012.

Wentz, F. J.: A well-calibrated ocean algorithm for SSM/I. Journal of Geophysical Research, 102(C4), 8703-8718, 1997.

Wentz, F. J., Hilburn, K.A., and Smith, D. K.: Remote Sensing Systems DMSP SSM/I Daily Environmental Suite on 0.25 deg grid, Version 7. Remote Sensing Systems, Santa Rosa, CA. Available online at www.remss.com/missions/ssmi. [Accessed 06 02 2017], 2012.

Atmos. Meas. Tech. Discuss., https://doi.org/10.5194/amt-2018-186
Manuscript under review for journal Atmos. Meas. Tech.
Discussion started: 20 June 2018

Atmospheric Measurement Techniques Discussions

Table 1. AIRWAVE v1 and v2 retrieval parameters for tropical summer atmosphere and along track configuration.

		α	β	δ	$\Delta\sigma_{NAD}$ 10^{-06}	$\Delta\sigma_{FWD}$ 10^{-06}	G_{NAD} 10^{-06}	G_{FWD} 10^{-06}	$\Delta\rho_{NAD}$ 10^{-06}	$\Delta\rho_{FWD}$ 10^{-06}
ATSR-1	V1	50.7	-49.7	1.65	1.49	2.41	-5.30	-8.82	—	—
	V2	1.72	-0.72	1.69	0.06	0.05	-6.59	-11.1	6.59	11. 2
ATSR-2	V1	50.5	-49.5	1.63	1.74	2.78	-6.36	-10.4	—	—
	V2	1.65	-0.65	1.67	0.07	0.04	-7.88	-13.1	7.89	13.2
AATSR	V1	53.1	-52.1	1.62	1.90	3.02	-7.06	-11.5	—	—
	V2	1.67	-0.67	1.66	0.08	0.05	-8.74	-14.5	8.77	14.6

Table 2. AIRWAVE TCWVs compared with SSM/I and ARSA stations. Absolute differences along with the standard deviations are reported for the global (all latitudes), equatorial (25S-25N), mid-latitude (25S-60° S and 25N-60° N) and polar (>60° N or >60° S) scenarios. Average values for the ATSR-1, ATSR-2 and AATSR are also provided.

		SSM/I-AIRWAVE			ARSA-AIRWAVE		
Instrument	Scenario	N.10^5	BIAS kg/m^2	STD	N.10^5	BIAS kg/m^2	STD
All	Global	3110	0.02	4.69	3.01	0.19	6.12
All	Equator	1560	-0.17	4.79	0.87	-0.70	6.60
All	Midlat	1380	0.07	4.84	1.80	0.49	6.10
All	Polar	170	1.32	3.51	0.35	0.86	4.59
ATSR-1	Global	190	-0.20	5.17	0.48	-0.71	6.24
ATSR-2	Global	1390	0.24	4.77	1.00	0.70	6.04
AATSR	Global	1520	-0.16	4.70	1.53	0.13	6.11

Atmos. Meas. Tech. Discuss., https://doi.org/10.5194/amt-2018-186
Manuscript under review for journal Atmos. Meas. Tech.
Discussion started: 20 June 2018

Atmospheric Measurement Techniques Discussions

Table 3. Impact of different error sources on AIRWAVE-v2 dataset.

Instrument	Scenario	Temp profile kg/m^2	wind (25 m/s) kg/m^2	HNO_3 kg/m^2	CFC-11 kg/m^2	CFC-12 kg/m^2	CO_2 kg/m^2	CFC-11 trends kg/m^2	CFC-12 trends kg/m^2	CO_2 trends kg/m^2	Noise kg/m^2
ATSR-1	Equatorial	3.6	-0.003	0.2	0.07	-0.07	0.003	-0.006	0.014	0.01	4.8
		(6.9%)	(-0.01%)	(0.4%)	(0.14%)	(-0.16%)	(0.006%)	(-0.01%)	(0.03%)	(0.03%)	(9%)
	Midlat	1.9	0.214								4.8
		(6.1%)	(0.69%)								(16%)
	Polar	0.6	0.448								3.0
		(3.9%)	(2.70%)								(18%)
ATSR-2	Equatorial	3.7	-0.008	0.15	0.05	-0.05	-0.003	0.015	0.009	-0.02	1.6
		(7.0%)	(-0.01%)	(0.3%)	(0.1%)	(-0.1%)	(-0.006%)	(0.03%)	(0.02%)	(-0.05%)	(3.1%)
	Midlat	2.0	0.230								1.6
		(6.6%)	(0.74%)								(5.2%)
	Polar	0.7	0.467								1.0
		(4.2%)	(2.8%)								(6.1%)
AATSR	Equatorial	3.7	-0.012	0.28	0.08	-0.07	0.006	0.01	0.01	-0.03	1.4
		(7.1%)	(-0.02%)	(0.56%)	(0.17%)	(-0.15%)	(0.01%)	(0.02%)	(0.02%)	(-0.07%)	(2.8%)
	Midlat	2.1	0.204								1.5
		(6.8%)	(0.66%)								(4.8%)
	Polar	0.7	0.447								0.9
		(4.3%)	(2.7%)								(5.6%)

Atmos. Meas. Tech. Discuss., https://doi.org/10.5194/amt-2018-186
Manuscript under review for journal Atmos. Meas. Tech.
Discussion started: 20 June 2018

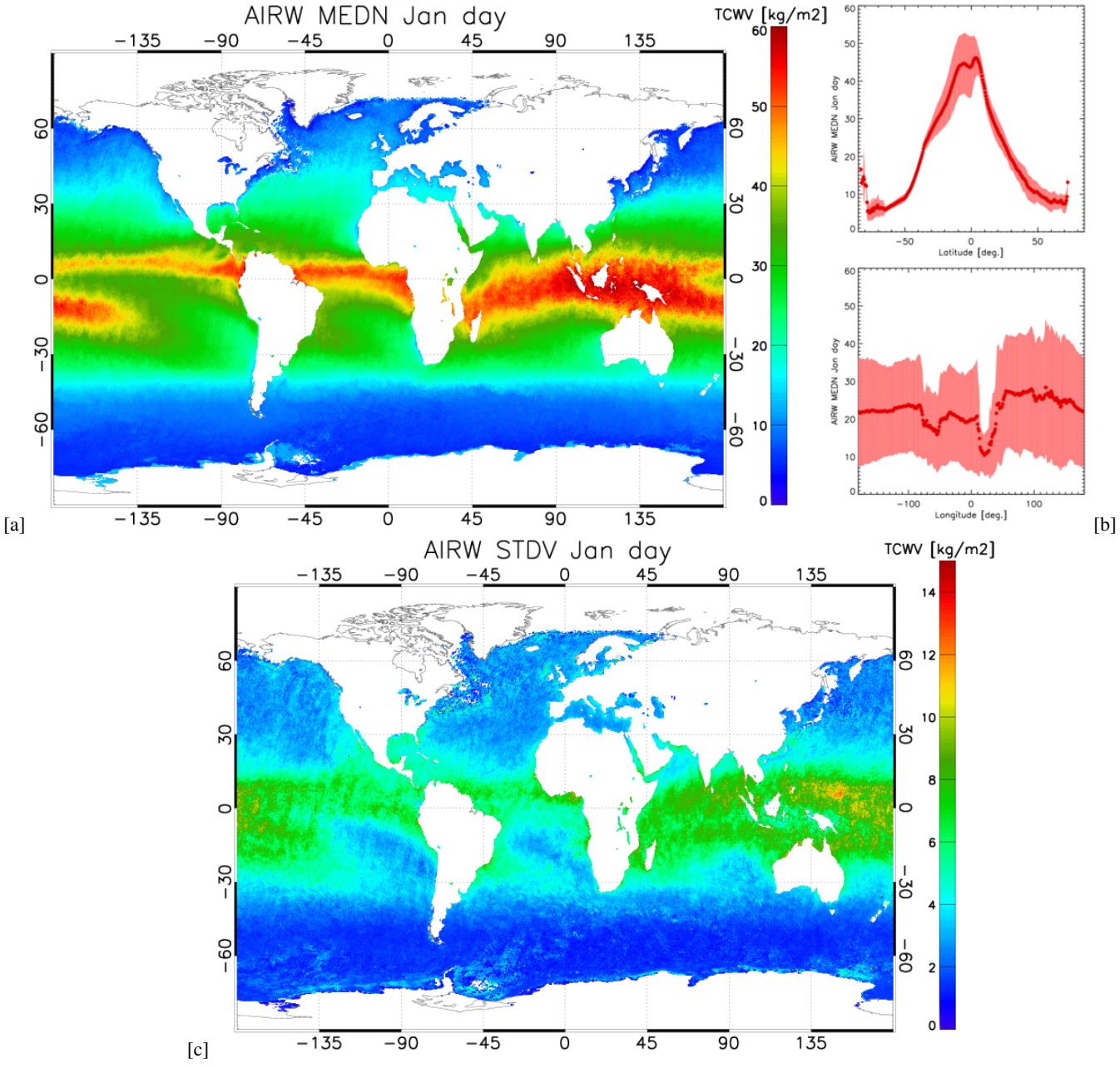

Figure 1. Climatology of daytime TCWV from AIRWAVEv2 dataset for January from 1991-2012, [a] Median TCWV. [b]: Top TCWV distribution as function of latitude (median and standard deviation). Bottom: TCWV distribution as function of longitude. [c]: Standard deviation.

Atmos. Meas. Tech. Discuss., https://doi.org/10.5194/amt-2018-186
Manuscript under review for journal Atmos. Meas. Tech.
Discussion started: 20 June 2018

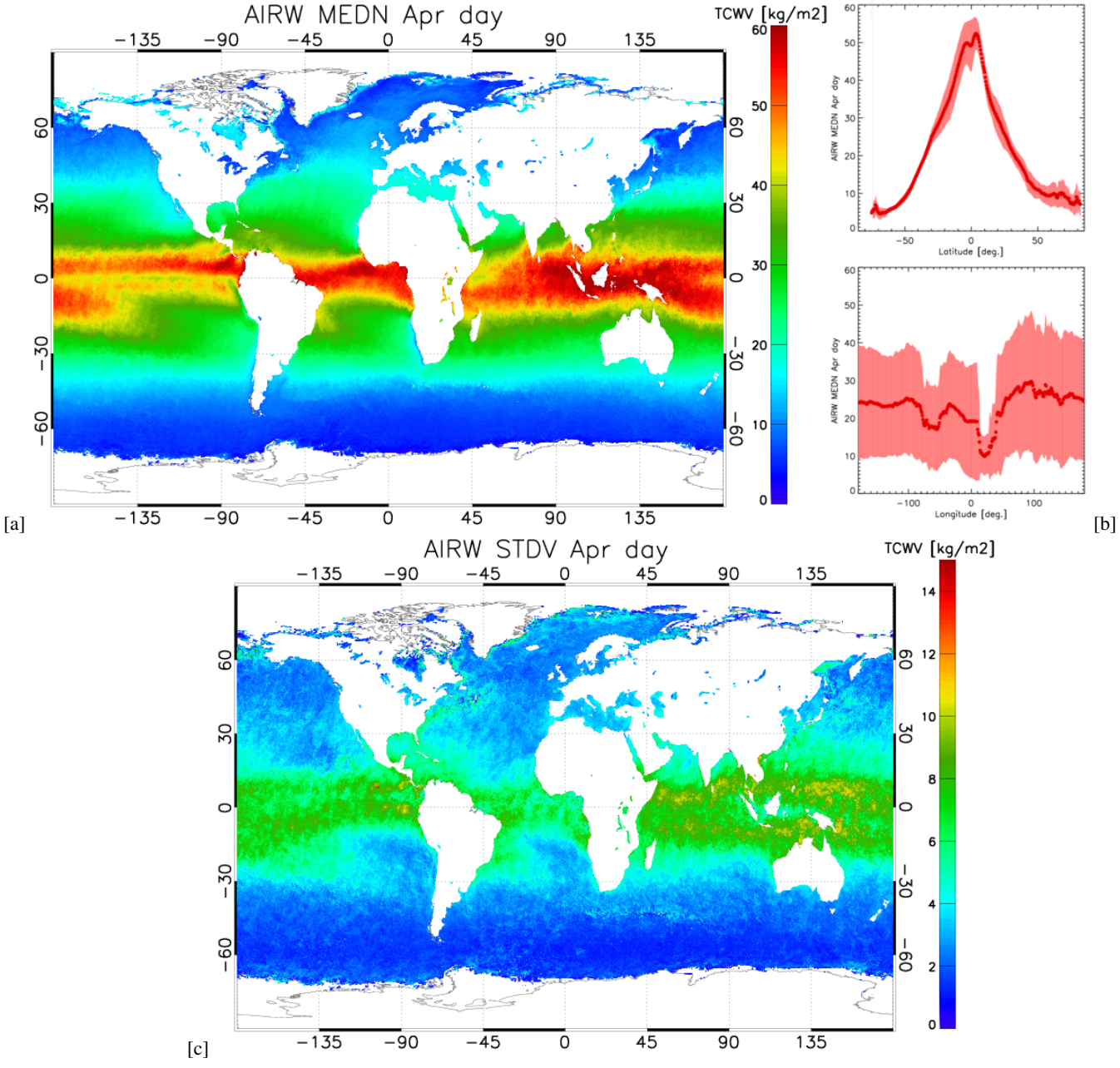

Figure 2. Climatology of daytime TCWV from AIRWAVEv2 dataset for April from 1991-2012, [a] Median TCWV. [b]: Top TCWV distribution as function of latitude (median and standard deviation). Bottom: TCWV distribution as function of longitude. [c]: Standard deviation.

Atmos. Meas. Tech. Discuss., https://doi.org/10.5194/amt-2018-186
Manuscript under review for journal Atmos. Meas. Tech.
Discussion started: 20 June 2018

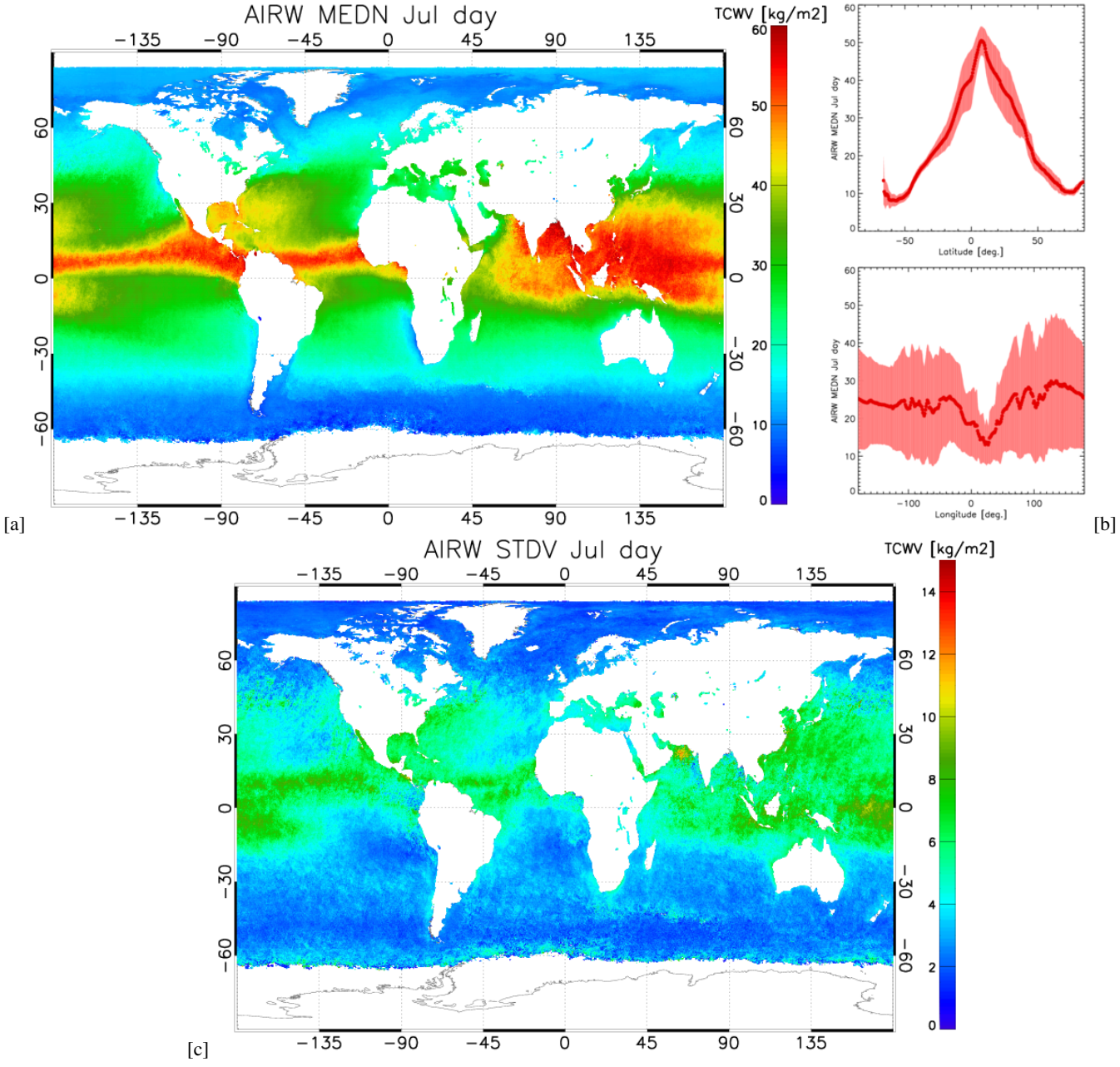

Figure 3. Climatology of daytime TCWV from AIRWAVEv2 dataset for July from 1991-2012, [a] Median TCWV. [b]: Top TCWV distribution as function of latitude (median and standard deviation). Bottom: TCWV distribution as function of longitude. [c]: Standard deviation.

Atmos. Meas. Tech. Discuss., https://doi.org/10.5194/amt-2018-186
Manuscript under review for journal Atmos. Meas. Tech.
Discussion started: 20 June 2018

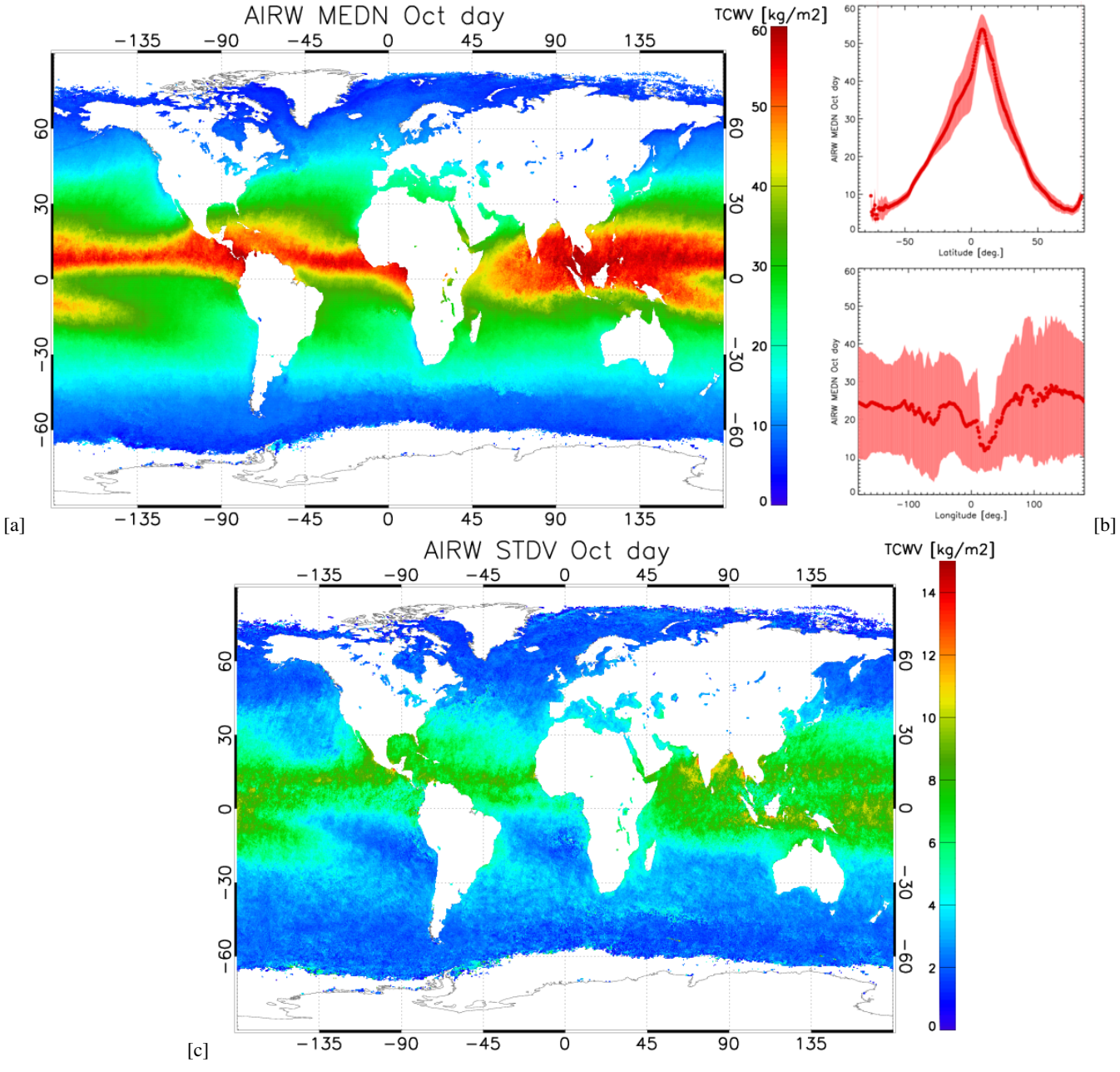

Figure 4. Climatology of daytime TCWV from AIRWAVEv2 dataset for October from 1991-2012, [a] Median TCWV. [b]: Top TCWV distribution as function of latitude (median and standard deviation). Bottom: TCWV distribution as function of longitude. [c]: Standard deviation.

Atmos. Meas. Tech. Discuss., https://doi.org/10.5194/amt-2018-186
Manuscript under review for journal Atmos. Meas. Tech.
Discussion started: 20 June 2018

Atmospheric Measurement Techniques Discussions

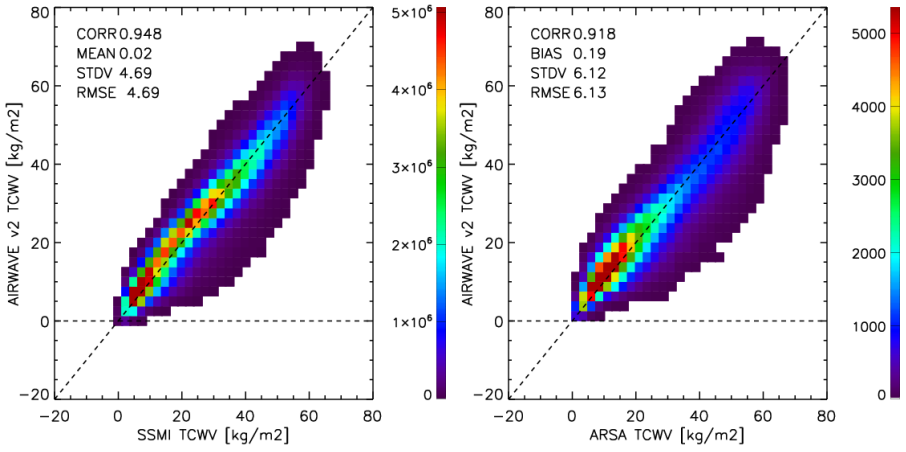

Figure 5. AIRWAVE TCWV vs SSM/I TCWV (left) or ARSA TCWV (right). The bin size is 2.5 kg/m^2. The colour scale indicates the number of elements of the histogram.

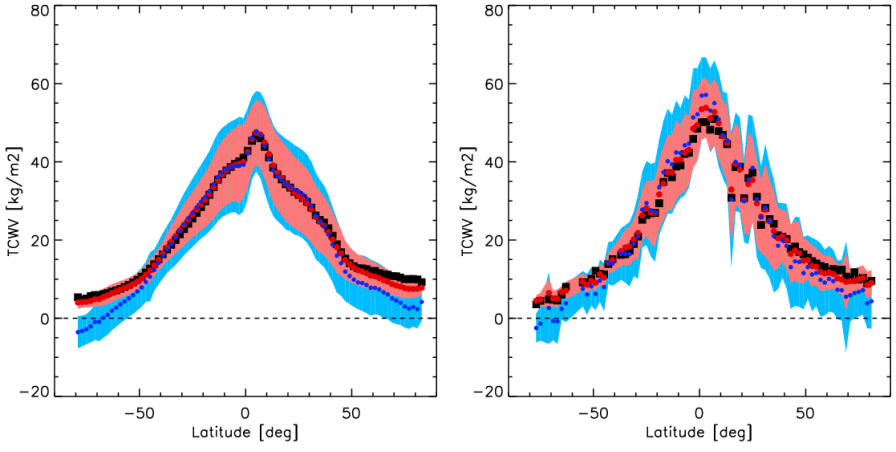

Figure 6. Zonal means of TCWV for AIRWAVEv1 (blue), AIRWAVEv2 (red) and correlative measurements (black): SSM/I (left) or ARSA (right). The data have been averaged in 2 degrees latitude bins. ARWAVE TCWVs standard deviations are also reported.

Atmos. Meas. Tech. Discuss., https://doi.org/10.5194/amt-2018-186
Manuscript under review for journal Atmos. Meas. Tech.
Discussion started: 20 June 2018

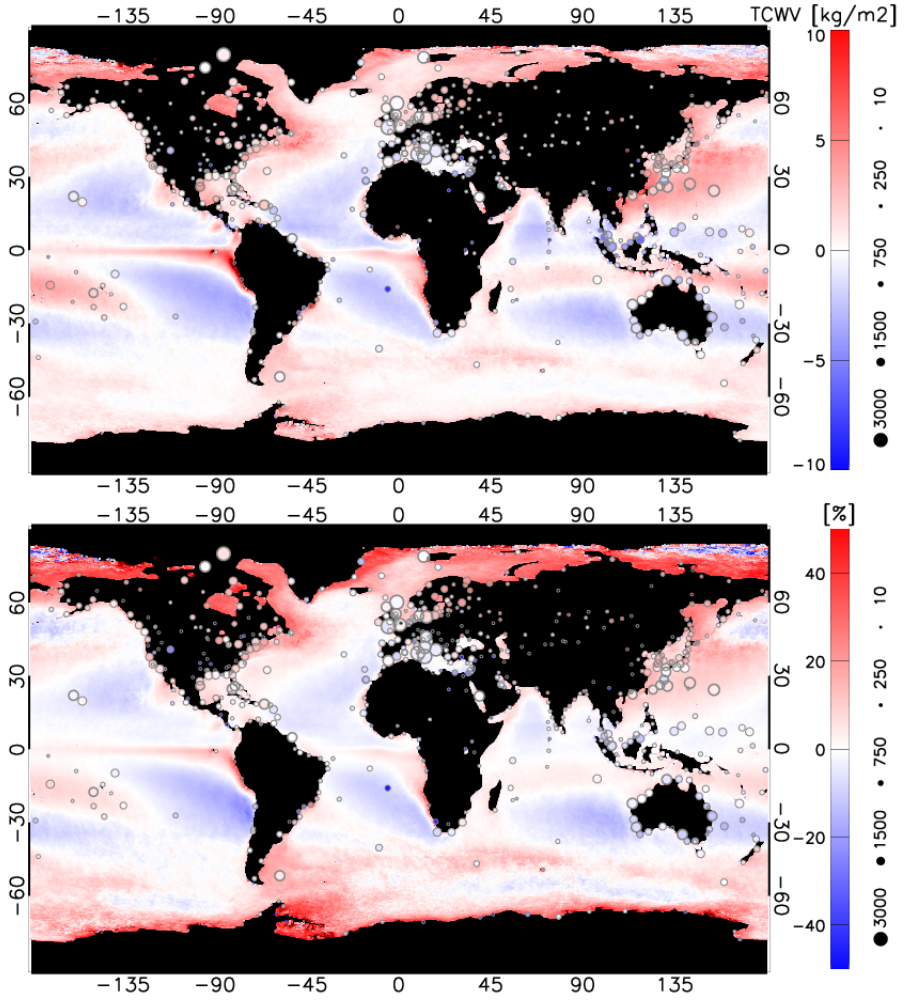

Figure 7. Average absolute (top) and relative (bottom) TCWV difference (SSM/I-AIRWAVE) at 0.25° × 0.25° spatial resolution. Average ARSA-AIRWAVE TCWV differences are overplotted with circles; the size of the symbols is proportional to the number of matches (see legend).

Atmos. Meas. Tech. Discuss., https://doi.org/10.5194/amt-2018-186
Manuscript under review for journal Atmos. Meas. Tech.
Discussion started: 20 June 2018

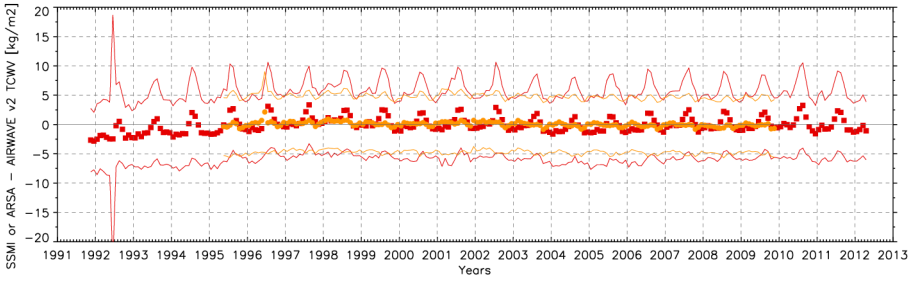

Figure 8. SSM/I-AIRWAVE TCWV (orange) and ARSA-AIRWAVE TCWV (red) monthly mean trends. The difference between the correlative measurements and AIRWAVE TCWV STDV is also reported.

Atmos. Meas. Tech. Discuss., https://doi.org/10.5194/amt-2018-186
Manuscript under review for journal Atmos. Meas. Tech.
Discussion started: 20 June 2018

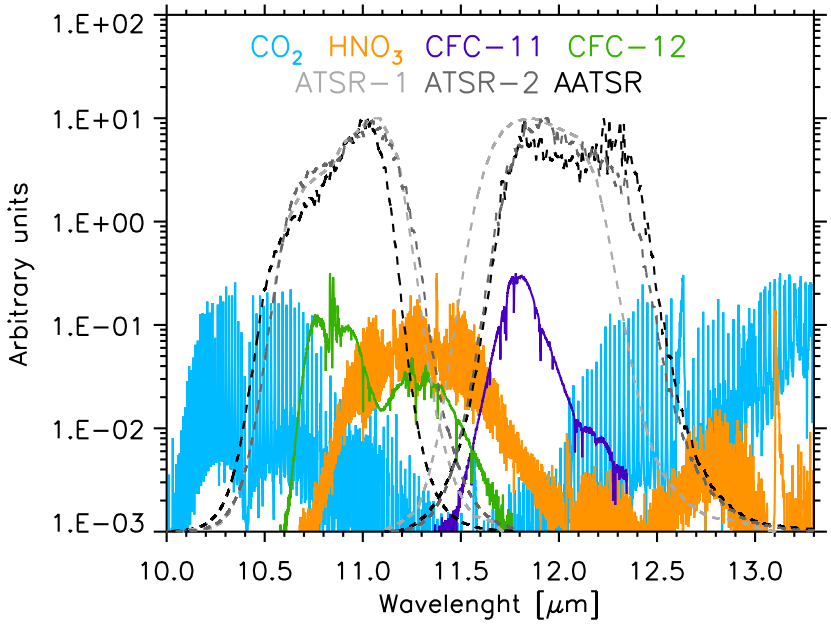

Figure 9. CO_2, HNO_3, CFCs spectral lines and ATSR filter functions (arbitrary units).